

Visualization and Quantification of Forced In-Plane Flow Through Deformed Porous Media*

HENRY L. FRIEDMAN, ROBERT A. JOHNSON**, VLADIMIR GUSEV,
ALEXANDER V. NEIMARK, DIANNE BUVEL, and DAVID R. SALEM

TRI/Princeton
Princeton, New Jersey 08542-0625

and

RICHARD S. PARNAS

Polymers Division
National Institute of Standards and Technology
Gaithersburg, Maryland 20899-001

Fluid flow in liquid molding processes and in other applications involving porous media is often characterized with a permeability tensor and modeled by d'Arcy's law. The permeability is a sensitive function of pore structure, which, in deformable materials, is influenced by compression and extension. The majority of previous permeability measurements on composite reinforcement fabrics did not account for deformations imposed on them by corners and curves in the mold. In the present study, transparent molds were designed with a single 90° bend in which the gap between plates was held constant throughout the flow path. Thus, the effects of fabric curvature on permeability were investigated independently of the effects of fabric compression in the thickness direction. A new experimental system was developed to visualize and quantify fluid flow in fabrics mounted in transparent molds. The reported measurements were conducted with fluid flowing through a (vertical) flat region of fabric, around the 90° curve, and then along a second (horizontal) flat region. Permeability was found to be reduced by the imposed curvature for a nonwoven polyester and three-dimensional woven glass fabric. We were able to quantify the effect of curvature on permeability for the former, but not for the latter because of an enduring, dominant nonlinear entrance resistance. For the glass, comparison of two flow rates indicates that the faster flow is characterized by a two stage filling process, whereas, at the slower rate, the liquid front fills all pores at the same time.

INTRODUCTION

Resin transfer molding (RTM) is an efficient and versatile process for producing fiber reinforced composite structures. In the basic process, a reactive pre-polymer is pumped into a mold with a preplaced dry fiber reinforcement. During and after mold filling,

polymerization occurs, and when the part has gained sufficient strength, it is removed. The chief advantage of RTM over other composite forming processes is the ability to make large parts of complex shape with lower cost equipment.

A number of test methods have been developed to assess the macroscopic fluid flow behavior in the porous reinforcement during mold filling (1). However, the measurements are often subject to large uncertainties, which are due to material nonuniformity and experimental artifacts that are difficult to control. D'Arcy's law,

$$\frac{Q}{A} = \frac{dL}{dt} = \frac{K\Delta P}{\eta L}, \quad (1)$$

*Part of this paper was presented at the American Society of Composites 13th Annual Technical Conference on Composite Materials, Baltimore, Maryland, Sept. 21-23, 1998. It appears in the conference publication: H. L. Friedman, A. V. Neimark, D. R. Salem, and R. S. Parnas, in *Proceedings of 13th Annual ASC Technical Conference on Composite Materials*, A. Vizzini, ed.

**Current address: Department of Chemical Engineering, Pennsylvania State University, University Park, PA 16802-4400.

is typically used to analyze the fluid flow experiments and characterize the reinforcement with a permeability tensor. An important point to note is that the liquid molding process is a multiphase flow process in which injected resin displaces air from the mold. Thus, d'Arcy's law, which describes saturated single phase flow, is not expected to fully describe the complex flow behaviors often observed in liquid molding. For example, in strongly wicking reinforcements the fluid infiltrates the material more quickly than expected, while in other cases the fluid infiltrates more slowly than expected from a knowledge of the d'Arcy permeability (2). These effects have been demonstrated and analyzed for flow in fibrous porous media (3, 4).

The permeability and overall flow behavior depend on the detailed structure of the porous media. Experimental results have shown unambiguously that the d'Arcy permeability can vary by more than a factor of 10 for materials of differing architecture at the same fiber volume fraction (5). Even small architectural details can have a large effect such as the six-fold increase in permeability observed in a unidirectional fabric when the crossing threads were removed (6).

The structure of the fiber reinforcements used in RTM is changed when the materials are forced to conform to corners and other bends in a mold. Mold filling simulations cannot account for such architectural effects on the flow behavior since very little permeability data exist for deformed media. In one case, the deformations of a continuous strand random mat and a 0/90 stitched fabric were modeled as shear deformation and permeability measurements were conducted on flat sheared fabric (7). In another case the flow be-

havior through fabric stretched over a cone was observed, and permeability values were inferred by matching a simulation to the experiment (8). Draping models are currently being used to approximate the fabric deformation in molds and crude correlations allow first order estimates of the change in permeability (7-9). However, 3-dimensional deformations are not properly accounted for in these treatments and it is unclear under what conditions significant errors may accumulate in such approximations. In an earlier report (10) we provided initial results on the effect of fabric curvature when a liquid is forced to flow through a confined fabric structure. Two transparent L-shaped cells with different gap thicknesses were made. The sketch of an L-cell is shown in Fig. 1. The cell was suspended in a reservoir that contained liquid, so that its liquid entry port was below the top of the liquid. The reservoir sat on the platform of a top loading balance. Liquid flow, which slowed as the run progressed, was controlled by evacuation and was monitored by mass balance readings corrected for buoyancy. The pressure drop driving the flow was measured with a differential pressure transducer. It was assumed that fabrics were saturated with liquid so that the flow length could be evaluated from the absorbed mass corrected for liquid density and cross-sectional area and porosity of the fabric. The overall permeability coefficient K of the fabric specimen was measured with water. The experimental techniques and analytical model used in the previous work were considered satisfactory for a non-woven polyester fabric but were thought to be less accurate in the case of a 3-dimensionally woven fabric. Despite the lower accuracy for the glass fabric, the

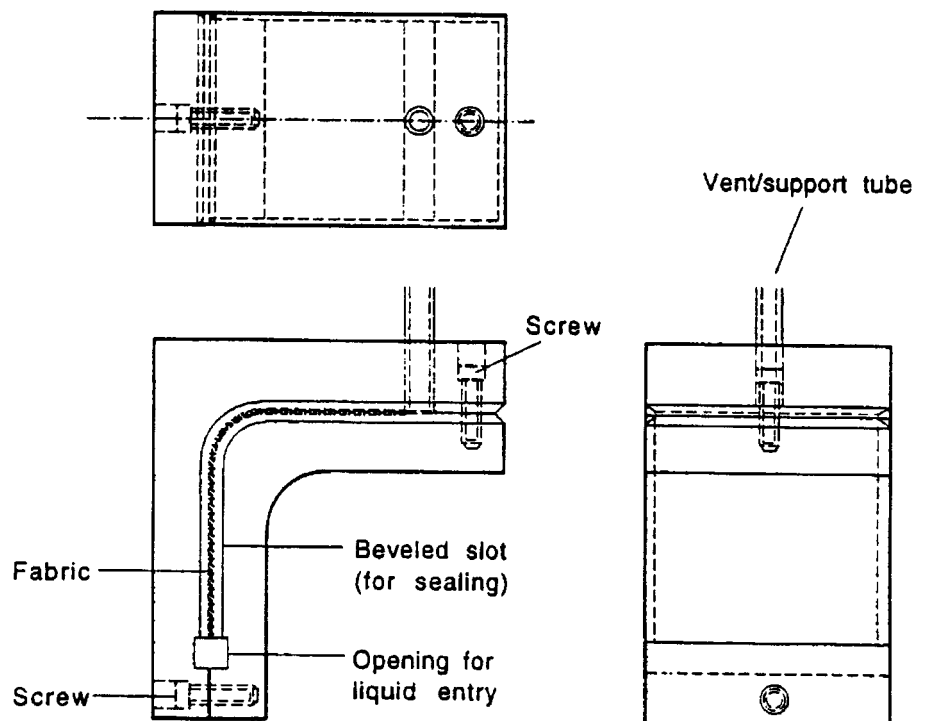


Fig 1. Sketch of the L-cell design that was used for in-plane flow measurements of fabrics by Liquid Air Displacement Analysis (10).

permeability was clearly reduced as a result of deformation in the curve for both types of fabrics.

In this paper, a new experimental setup is used, involving visualization of fluid flow, and a number of improvements in data interpretation are reported. New data are presented for polyester and 3-D woven glass fabrics. The effect of flows around curves of several radii, and the influence of flow rate on pore-filling behavior is examined for the glass fabrics.

EXPERIMENTAL

Cells, Fluid Injection, and Pressure Measurements

A sketch of the new type of L-cell, together with the complete flow system used for this study is shown in Fig. 2. The inner part of the cell, which is made of brass for rigidity, contains the liquid entry and exit ports, and the female threads for port hardware and assembly screws. The outer part, which is made of ICI Acrylics Lucite®, and is approximately 5 cm thick for rigidity, contains a uniform 3.18 mm thick gap for fabric specimens and a tapered channel from the entry port to the liquid entry edge of the fabric. Cells with inner radii of curvature of 4.76 mm, 7.94 mm, and 11.11 mm have been fabricated.

The shape of these cells and the orientation of the screws, make it difficult to assemble them accurately and reproducibly by hand, so an assembly jig was fabricated to control the relative movements of the mold parts.

Polysiloxane adhesive is used to seal the edges of the fabric and the beveled edges of the cell between the brass and Lucite and single faced tape is used to seal the openings for the screws. The adhesive is applied while the cell is partly evacuated to draw it as close to the fabric as possible. The success of sealing is tested by seeing if the cell holds vacuum while the adhesive is fluid. Additional adhesive is applied to seal leaks.

The other components of the measurement system are also shown in Fig. 2. Liquid is injected with a piston/cylinder pump driven by a computer controlled stepper motor. Air is removed from liquid in the pump, differential pressure transducer, and feed line before the liquid is allowed to contact the fabric specimen.

Flow Visualization

Black and white digital cameras with resolutions of 242 × 753 pixels are focused on the flat vertical and horizontal surfaces of the fabric specimen, which are illuminated with variable intensity fiber optic lamps.

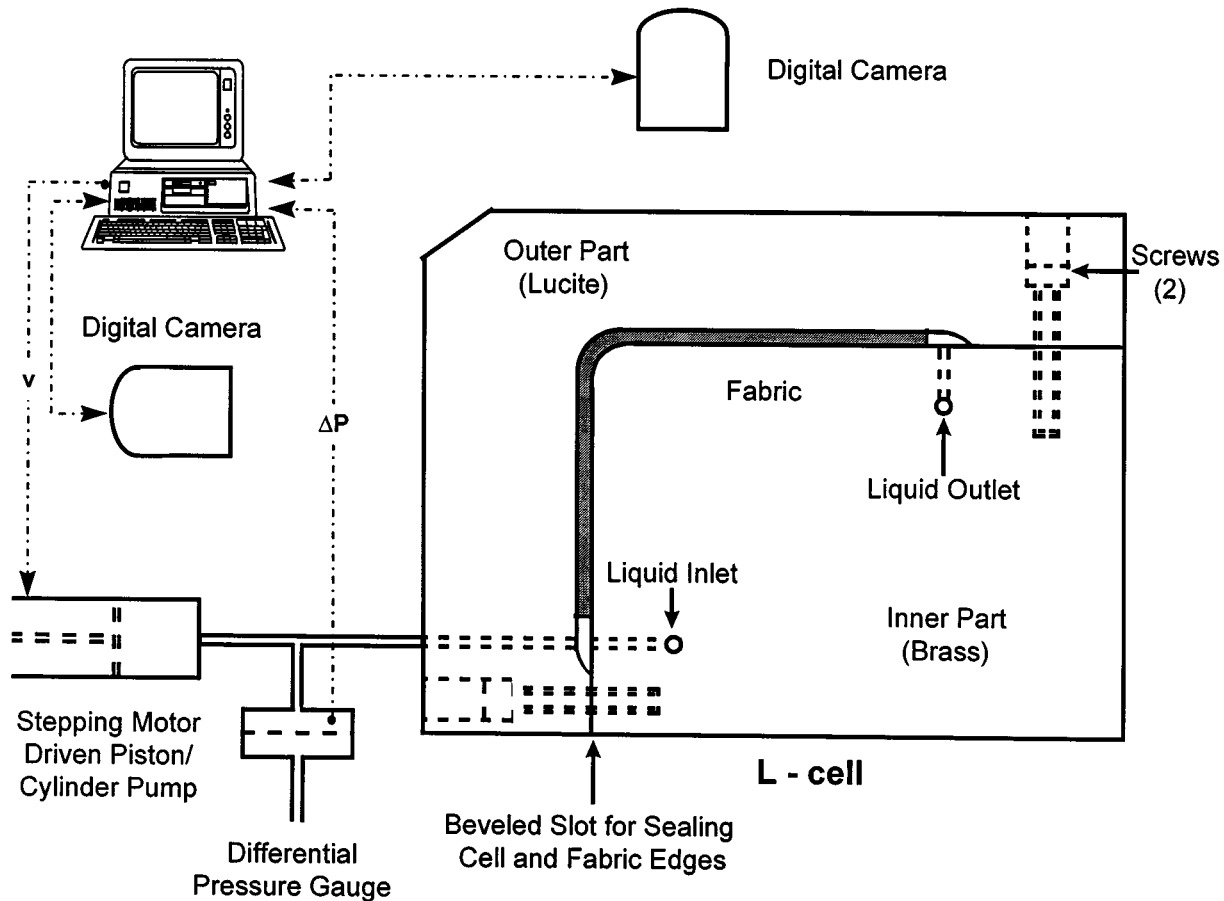


Fig. 2. Sketch of the current L-cell measurement system.

We monitor images in both flat regions, together with readings of the pressure transducer, as flow progresses, but do not monitor the liquid in the curve at this time. The current software, which uses National Instruments LabVIEW® in the Windows 95® environment, obtains pairs of images in both flat regions at preselected intervals, examples of which will be shown below. Data acquisition times are not exact, so clock times are stored. The minimum interval for obtaining pairs of images is ~ 1.25 s.

Air Permeability Measurements

Air flow resistance measurements were also made with the TRI - ART™ Air Resistance Tester (11) before liquid permeability measurements were performed. The liquid exit port of the L-cell is attached to the entrance tube of the ART so that air is drawn through the fabric in the same direction as liquid flows during liquid permeability measurements.

MATERIALS

The same nonwoven polyester (10) and 3-dimensional woven glass fabrics (2, 10), which were studied earlier, were examined with the new system. Deionized water was used for both materials, but the glass fabric is so dense that it was not possible to visualize the flow of water at its surface. Visualization was accomplished by use of a 0.01% aqueous solution of Rhodamine B dye with the aid of narrow band 540 nm filters. The surface tension of this solution was 62 dynes/cm, as compared to 69 dynes/cm for the pure water.

Glass fabric specimens were bias cut into rectangular strips with a printer's paper cutter, with narrow thin transparent single faced tape on both surfaces to stabilize cut edges. Splayed edge fibers were trimmed with a razor blade.

IMAGE ANALYSIS

Introduction

During the fluid flow experiment the images of the fluid in a fabric are taken by the digital computer cameras and saved in the 8-bit gray scale TIFF format. In other words, each image is a two-dimensional 243 by 756 array of integers in the range of 0 to 255, representing the light intensity observed in the corresponding pixel. Two indexes of each of the integers in the array represent the x and y coordinates of the pixel position. The program, written in LabVIEW® 4.1 and C++ (Microsoft VC++ 5.0), analyzes input data in order to gain fundamental information on fluid flow in these structures. The output of this program is in the form of video and several graphs that are updated dynamically. The basic stages of the algorithm are described in the following sections.

Subtracting Background

The images obtained during the measurements represent very complex intensity fields, which need to be

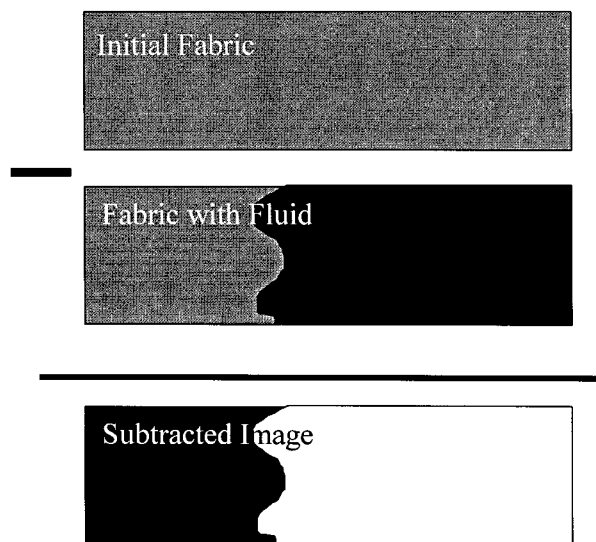


Fig. 3. Top image (fabric before liquid injection); middle image (fabric during liquid injection); bottom image (middle image minus top image).

simplified before analysis. The first step, which consists of subtracting the background from all subsequent images, is illustrated in Fig. 3.

As a result of this procedure, the regions with no fluid become absolutely black (0 intensity), while the parts that are filled with fluid are composed of pixels with the varying light intensity. The intensity of the light is a function of the amount of fluid at a particular location, i.e., the more fluid the greater the intensity.

Binarization With Preservation of Luminosity

In order to determine the position of the front, it is necessary to decide the threshold level of luminosity at which a particular pixel is to be considered filled. The threshold level is evaluated during data processing as illustrated in Fig. 4, which is a plot of lumi-

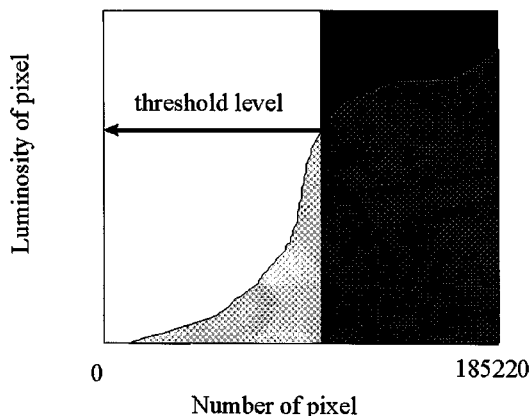


Fig. 4. Sketch of the protocol to automatically choose the position of the liquid front along a longitudinal pixel based on conservation of luminosity.

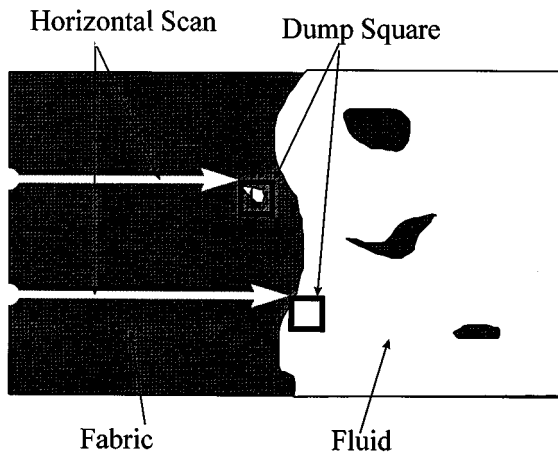


Fig. 5. Protocol to eliminate atypical features of the binary image for assignment of the location of the liquid front.

nosity of each pixel in the current image in order of increasing intensity. The area of the darkened rectangle is equal to that under the curve. The threshold level is defined as the luminosity at the left boundary line of the darkened rectangle. The intensity of each pixel whose luminosity is below the threshold is reduced to zero, while the intensities of the others are elevated to 255 in a binary image of the absorbed liquid (see Fig. 7). Thus the total luminosity of the image is conserved. (If the luminosity of the subtracted image is a monotonic function of the quantity of fluid in the fabric, the conservation of the balance of luminosity is equivalent to the conservation of the quantity of fluid as reflected by the binary image of the fabric.)

Front Position Determination with Filtering and Quantification of Fluid Patterns

Local positions of the fluid front are determined from the binary image by scanning in a row-by-row fashion across the fabric in the reverse direction of fluid flow, as illustrated in Fig. 5. The position of the first pixel with the light intensity value of 255 along each line is accepted as its local front. Small "run-away" fluid droplets, which are not characteristic of the position of the main body of the fluid, and/or imperfections in the data image can be disregarded by dumping them, based on their size in both x and y directions. The dumping factor (the size of the dump square) is adjustable, and is chosen based on experience. The dumping procedure is automated. The result of the scanning procedure is illustrated in Fig. 6.

The average front position and its standard deviation are evaluated from the quantified individual longitudinal pixel values determined across the fabric.

Typical Flow Analysis

Figure 7 shows the on-screen presentation during an analysis of absorption in the vertical region of the 3-D glass weave with dyed water. The top left image is

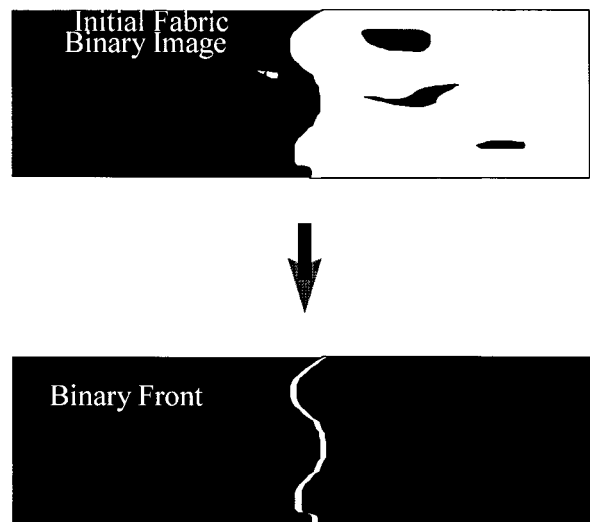


Fig. 6. Top image (binary image before elimination of atypical features); bottom image (binary image of the position of the liquid front).

the raw image taken by the camera during the measurement (the direction of flow is from right to left). Below it is the result of subtraction of the background before flow started. Next is the binary image, and last, the outline of the absorption front and the straight line that shows the location of the average position of the front. The upper part of the right panel contains tools to perform and control the analysis. The middle graph shows image-by-image plots of total luminosity (the center line), average front location (the upper line), and standard deviations across the front (the lower line). The bottom plot is an image-by-image bar graph of luminosity vs. pixel location along the entire image in the direction of flow.

RESULTS

Nonwoven Polyester

One specimen of polyester was measured in the cell with medium curvature (7.94 mm) with deionized water at a flow rate of 0.2 cm³/s. Digital images were obtained as frequently as possible, i.e., at ~ 1.25 s intervals. A plot of ΔP vs. time is shown in Fig. 8. Pressure increased as liquid rose in the flat vertical region because of increased viscous drag and increased hydrostatic pressure due to gravity. Pressure increased further when liquid was in the curve, but at a reducing rate due to the decreasing contribution of gravity with increased length of absorbed liquid. Pressure continued to rise in the flat horizontal region due to increased viscous drag, but at a slower rate than in the vertical region because the gravitational contribution did not change. A plot of the absorbed average liquid length L (from digital images) vs. time is shown in Fig. 9. It is nearly linear, as it should be, for liquid injection at a constant flow rate. Figure 10 is the plot of ΔP vs. L of the data in Figs. 8 and 9. The nearly linear

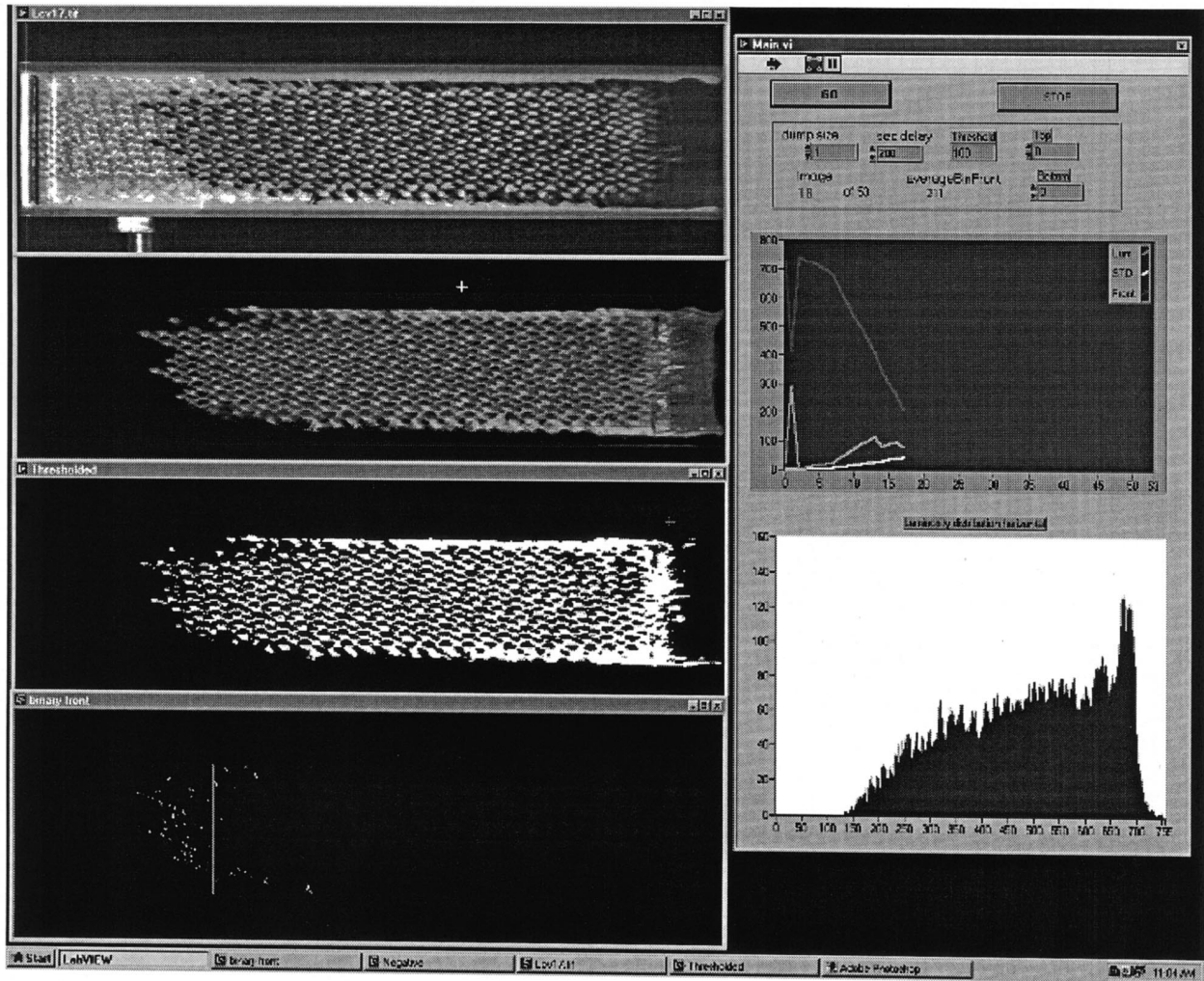


Fig. 7. Monitor screen during the analysis of forced in-plane flow.

sections in the two flat regions were analyzed to obtain permeability coefficients in the following way. The value of K_h in the horizontal region was determined from d'Arcy's law expressed as

$$K_h = \frac{Q\eta}{A(d\Delta P/dL)}, \quad (2)$$

where $d\Delta P/dL$ is determined from a linear regression

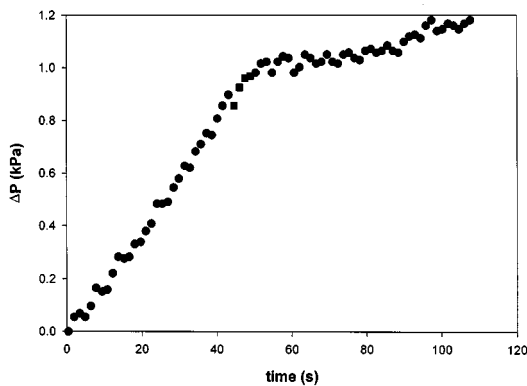


Fig. 8. ΔP vs. time for the nonwoven polyester fabric in the L-cell with the 7.9 mm inner radius with H_2O at $Q = 0.2 \text{ cm}^3/\text{s}$. (Square points represent flow in the curve.)

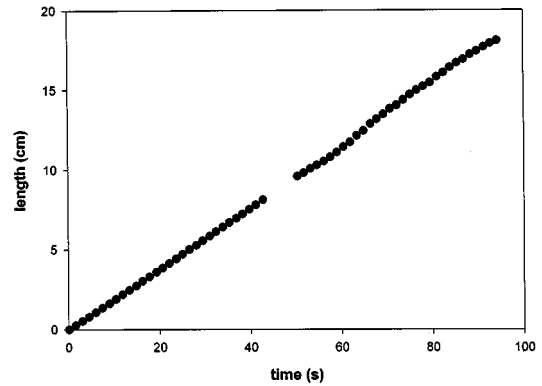


Fig. 9. Average length of the absorption front vs. time for the nonwoven polyester fabric in the L-cell with the 7.9 mm inner radius with H_2O at $Q = 0.2 \text{ cm}^3/\text{s}$.

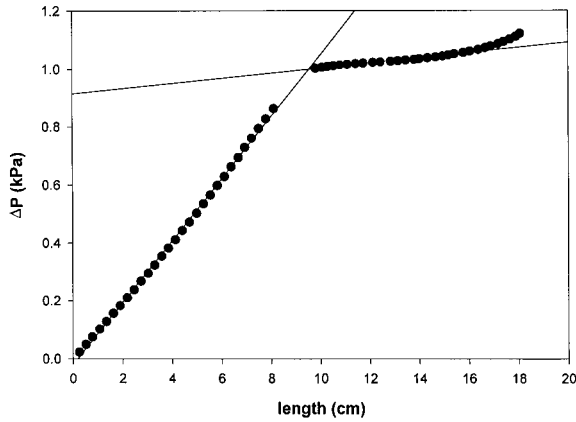


Fig. 10. ΔP vs. average length of the absorption front for the nonwoven polyester fabric in the L-cell with the 7.9 mm inner radius with H_2O at $Q = 0.2 \text{ cm}^3/\text{s}$.

fit in that region. For the vertical region, the value of K_v is expressed as

$$K_v = \frac{Q\eta}{A[(d\Delta P/dL) - \rho g]} \quad (3)$$

It is necessary to subtract ρg ($\rho g = 98.07 \text{ Pa/cm}$) from $d\Delta P/dL$ to account for the effect of gravity in the vertical region. The values of K_v and K_h were estimated as 1.81×10^{-5} and $1.78 \times 10^{-5} \text{ cm}^2$, respectively. Their agreement is reasonable for flat regions with the same gap width.

The evaluation of the permeability of the curved region, K_c , was based on the facts that Q is constant and when liquid reached the end of the fabric, we know the exact fluid flow lengths in the flat vertical, curved, and flat horizontal regions. Therefore, Eq 1 can be expressed as

$$v = \frac{Q}{A} = \frac{K_t \Delta P_t}{\eta L_t} = \frac{K_v \Delta P_v}{\eta L_v} = \frac{K_c \Delta P_c}{\eta L_c} = \frac{K_h \Delta P_h}{\eta L_h} \quad (4)$$

where the ΔP terms are net values, i.e., hydrostatic pressures are eliminated. Since the three zones are resistances in series

$$\Delta P_t = \Delta P_v + \Delta P_c + \Delta P_h \quad (5)$$

Combining and rearranging parts of Eqs 4 and 5, results in

$$K_c = \frac{L_c}{\frac{L_t}{K_t} - \frac{L_v}{K_v} - \frac{L_h}{K_h}} \quad (6)$$

The overall value of K_t was determined from

$$K_t = \frac{Q\eta L_t}{A(\Delta P - \rho g h_t)} \quad (7)$$

For this measurement, the value of K_c is 5.14×10^{-6} , in agreement with our earlier observations (10), and is a factor of about 3.2 less than the permeabilities in the flat regions.

3-Dimensional Woven Glass Fabrics

Eight specimens of glass were examined altogether, two each in all three cells at a flow of $0.2 \text{ cm}^3/\text{s}$ and one each in the cells with the smallest and largest curves at a flow of $0.02 \text{ cm}^3/\text{s}$. Images were obtained as frequently as possible for faster flow and at $\sim 4 \text{ s}$ intervals for the others.

Fast Flow

For this material, a sharp pressure increase always occurs at liquid contact. (Such increases were also ob-

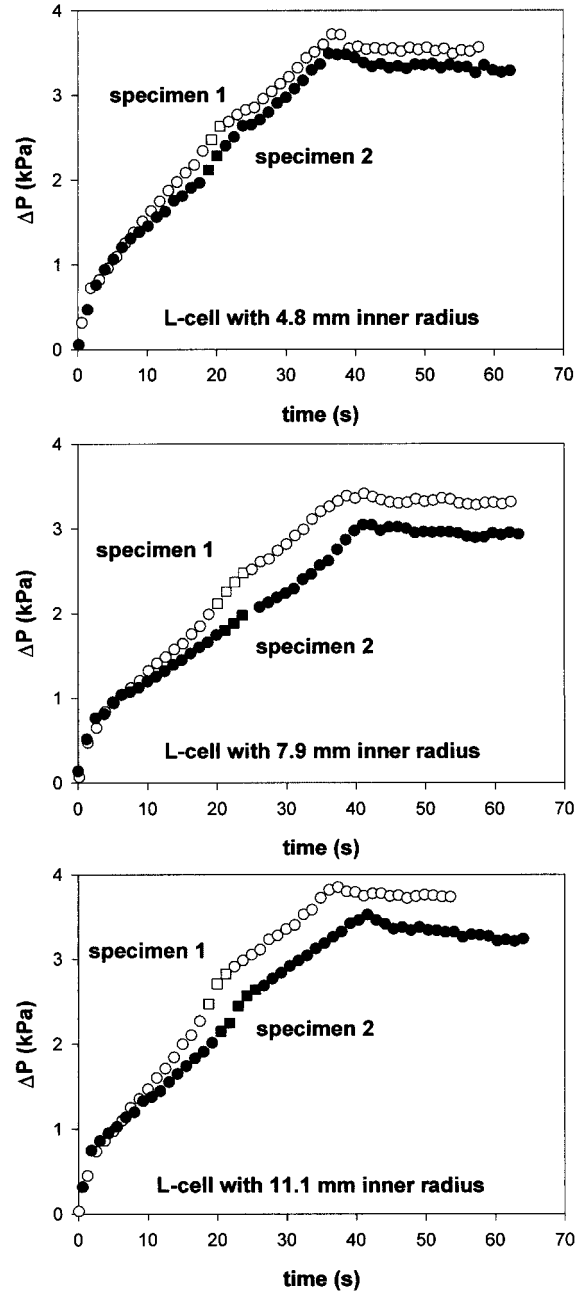


Fig. 11. ΔP vs. time for the 3-dimensional woven glass fabrics in L-cells with different curvatures with H_2O at $Q = 0.2 \text{ cm}^3/\text{s}$. (Square points represent flow in the curve.)

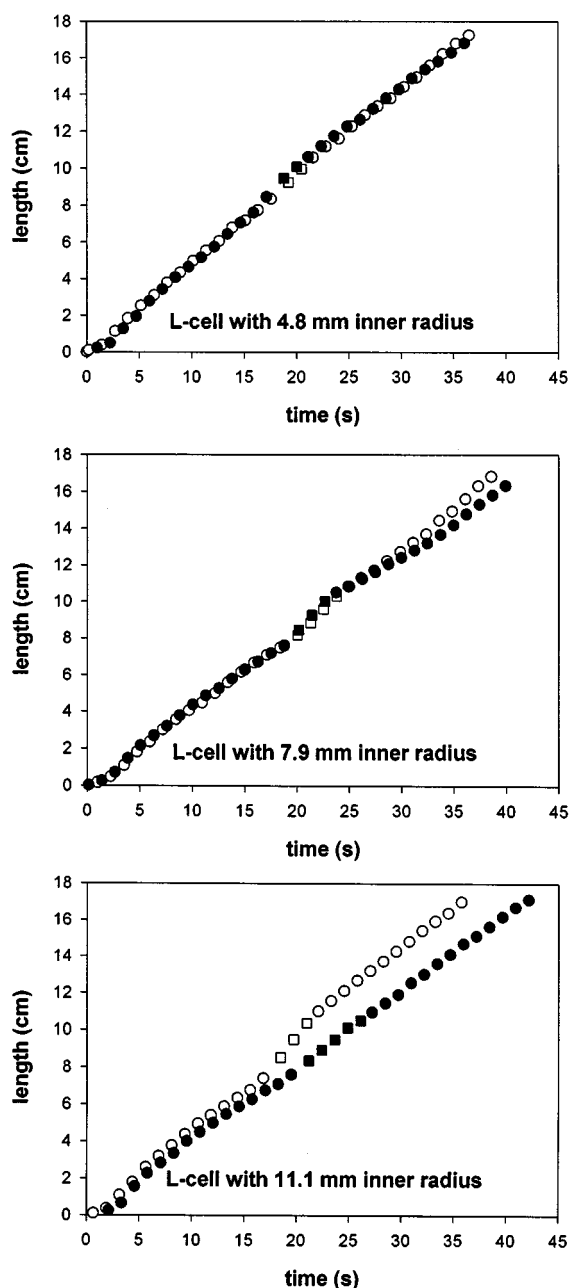


Fig. 12. Average length of the absorption front vs. time for the 3-dimensional woven glass fabrics in L-cells with different curvatures with H₂O at Q = 0.2 cm³/s. (Square points represent flow in the curve.)

served by Parnas *et al.* (2) for these fabric structures when liquid was forced into their vertical molds from below the fabric. We did not observe a significant rise for polyester.) Contact time and ΔP are estimated from the intersection of curve fits before and after this distinct event. Thus, they are even more accurate than those obtained by comparing images. All subsequent values of ΔP and time were normalized relative to the contact values, which were assumed to be zero. Plots of ΔP vs. time for all six measurements are shown in Fig. 11. For each measurement, pressure rose to ~ 0.6 kPa within a few seconds after the liquid entered this dense fabric. Rapid rises were followed by slower comparatively linear increases in ΔP , as were also found by Parnas *et al.* (2). (As will be shown, the magnitude of this rise seems to be independent of flow rate. While we cannot explain the reason for it, we speculate on possible causes in the **Discussion** section.) Values of ΔP increased more rapidly when liquid reached the curve, which showed that flow resistance increased there, consistent with our earlier observations (10) for this fabric. Rather linear increases of ΔP resumed somewhat after the liquid front was past the curve. The value of ΔP decreased slightly and became nearly constant when liquid left the fabric. Comparison of pairs of measurements that were performed with different specimens in the same cell showed some differences.

Figure 12 contains nearly linear plots of L vs. time for the same measurements in Fig. 11. Velocities from linear least squares regression fits are shown in Table 1. Their average is 0.453 cm/s $\pm 10\%$. Velocities would be ~ 0.34 cm/s if the pores were completely filled. Departures from linearity can be attributed to heterogeneities in fabric structure and some errors in evaluation of L . (Since we do not measure the position of the front in the curve, it was interpolated from L vs. t values in the nearby vertical and horizontal regions.)

Plots of ΔP vs. L for the data in Figs. 11 and 12 are shown in Fig. 13. Their shapes are similar to Fig. 11, because velocities were nearly constant. Since the plots were nearly linear in the flat regions, after the early pressure rise seemed to end in the vertical region and somewhat after the liquid front was past the curve in the horizontal region, linear regression fits were used to evaluate $d\Delta P/dL$ and values of K_v and K_h from them through Eqs 2 and 3. Values of overall liquid and air K_i 's were calculated with Eq 7, but they

Table 1. Average Linear Liquid Velocities and Permeability Coefficients of 3-Dimensional Woven Glass Fabrics in L-cells With H₂O at Q = 0.2 cm³/s.

Inner Radius, mm	Specimen No.	Avg. dL/dt , cm/s	$10^6 \times K_v A$, cm ⁴	$10^6 \times K_h A$, cm ⁴	$10^6 \times K_i A$, cm ⁴	liquid	air
4.8	1	0.477	1.53	1.07	1.19	1.33	
4.8	2	0.484	3.44	1.00	1.29	1.44	
7.9	1	0.441	2.59	1.26	1.40	1.60	
7.9	2	0.409	3.88	0.93	1.56	1.80	
11.1	1	0.495	1.28	1.23	1.18	1.30	
11.1	2	0.414	1.71	1.31	1.24	1.44	

may be inaccurate because initial pressure rises were included in values of ΔP . Since there was some uncertainty in the width of the specimens due to splaying, and its value is essentially constant, permeabilities are reported as the product of K and A . (The value of $A \sim 1.21 \text{ cm}^2$.) (Overall air permeability values of $K_t A$ were determined from measurements at several flow rates, a typical plot for which is shown in Fig. 14. Air permeability tends to decrease with increasing flow rate because of kinetic energy and frictional losses at faster air velocities (12). Since the air pumping system

that was used produced a minimum flow rate of $\sim 0.28 \text{ cm}^3/\text{s}$, air permeabilities at liquid flow rates were estimated from curve fits by extrapolation.)

Values of $K_v A$, $K_h A$, and $K_t A$ are also shown in Table 1. Values of $K_v A$ are significantly larger than $K_h A$ for every specimen. It is troublesome that they are so different from each other, because one would expect them to be nearly the same in flat regions with equal gaps, as they were for the polyester. While the values of $K_v A$ are so variable, those of $K_h A$ and $K_t A$ are relatively similar for all of the measurements. These factors suggest that this analysis does not properly account for the cause and duration of the pressure rise accompanying liquid entry, at least in the vertical region, so values of $K_v A$, in Table 1, are too large. By assuming $A \sim 1.21 \text{ cm}^2$, we can estimate values of K_h and K_t from KA values in Table 1, as ranging from ~ 7.7 to 10.8×10^{-7} and ~ 9.8 to $12.9 \times 10^{-7} \text{ cm}^2$, respectively. Parnas *et al.* (2) measured saturated values for flat vertical fabrics of this type, in the same flow direction as used in this study, which ranged from 6.3 to $10.3 \times 10^{-7} \text{ cm}^2$, in good agreement with our K_h 's and K_t 's. Our values may be slightly larger than theirs because of unsaturation. More about the comparison between our K_t 's and their saturated values, will be said below. Air values of $K_t A$ were a little larger than liquid values, possibly because initial pressure rises could not be taken into account for liquid values.

We believe that the $K_t A$ values are accurate, and the real $K_v A$'s are quite close to them. We feel, however, that it is risky to estimate values of $K_c A$ with Eq 7 because we are unsure about the accuracy of $K_t A$'s.

As cited earlier, Parnas *et al.* (2) observed similar pressure rises when liquid contacted this type of fabric during their unsaturated measurements. Since they did not measure the position of the liquid front, they estimated it from the flow rate, time, cross-sectional area, and volumetric porosity, having assumed that the pores were saturated. Cumulative values of K were calculated from d'Arcy's law expressed as

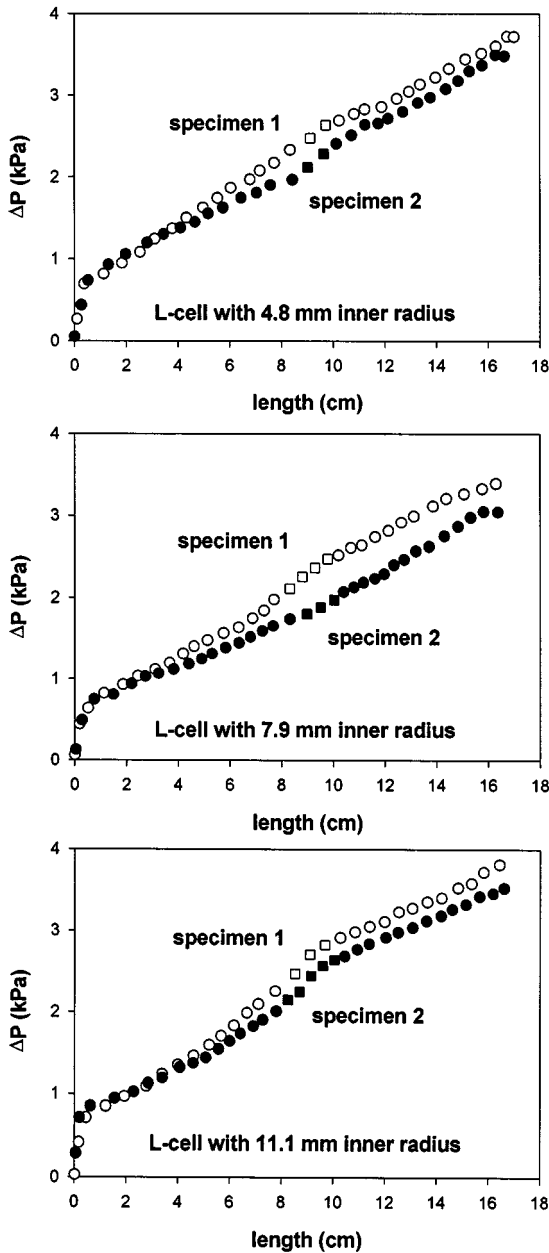


Fig. 13. ΔP vs. average length of the absorption front for the 3-dimensional woven glass fabrics in L-cells with different curvatures with H_2O at $Q = 0.2 \text{ cm}^3/\text{s}$. (Square points represent solid flow in the curve.)

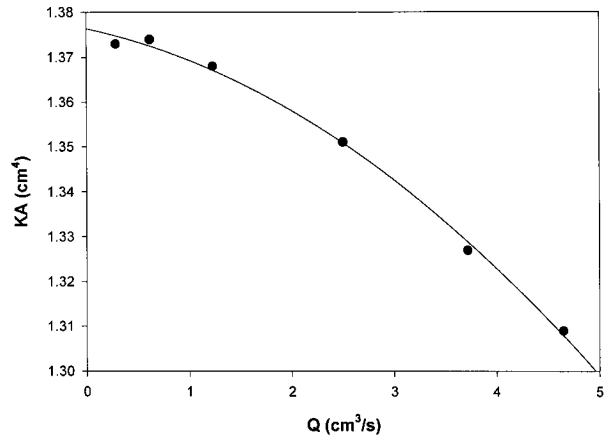


Fig. 14. Air permeability of the 3-dimensional woven glass fabrics in the L-cell with the 4.8 mm inner radius.

$$K = \frac{Q\eta L}{A(\Delta P - \rho gh)}, \quad (8)$$

where $h = L$, because their molds were vertical. They found that initial values of K were ~ 30 to 50% of saturated ones, that they increased as flow progressed, and eventually tended to level off. Maximum values exceeded saturated ones by ~ 20 to 60% . They attributed the rise of K to initial flow between the tows. Channels within the tows were thought to be blocked by air, and to become increasingly available to liquid penetration as the pressure of liquid increased.

We calculated equivalent values of K from the measured values of L . In the vertical region $h = L$, in the curve $h = L_v + r\sin\theta[180(L - L_v)/\pi r]$, and in the horizontal region $h = h_h$. Values of K derived from Eq 8, for some of the data in Figs. 11 and 12, are plotted vs. L in Fig. 15. For all of these measurements, values of KA were very small when liquid contacted the fabric, increased as liquid climbed in the vertical region, and tended to become nearly constant by the time it reached the curve, similar to the observations of the earlier study. Permeabilities in the flat regions differed little between cells or specimens. They, and our estimates of K_v , are somewhat larger than the saturated values of Parnas *et al.* (2); however, they are consistent with the larger later unsaturated values reported in the earlier study.

Attempts to analyze absorption in the flat vertical region as the result of the sum of a constant entry resistance and that proportional to L were unsuccessful, so the initial pressure rise does not appear to be caused by a simple entrance effect. In addition, wettability and wicking measurements showed that the fluid/fiber interaction was lyophilic, so that the pump

did not need to apply extra force for the liquid to overcome negative capillary pressure effects. It is not possible to quantify the effect of the curve from cumulative values of K because the curved portion represents only a small part of the total length of the specimen, and the cause of the apparent increase in permeability has not necessarily terminated by the time the liquid reaches the curve, or even the end of the specimen. Furthermore, analysis of the effect of the curve is complicated by nonuniform fronts and the short curve lengths, which cause parts of the front to be in and out of the curve at the same time.

Slow Flow

Plots of ΔP vs. time for both of these measurements are shown in Fig. 16. (Increased noise in pressure values compared to those in Fig. 11 are attributed to lower signal-to-noise ratios for the slower flow rates.) Each showed the relatively rapid rise of pressure when liquid contacted the fabric, which was of the same magnitude as for flows that were ten times larger, as shown in the plots of ΔP vs. time for the two flow rates in the vertical region of the same cell in Fig. 17. Differences in their slopes are, however, consistent with flow rates. There was a significant increase in ΔP when liquid reached the curve of the 4.8 mm cell, which showed a significant reduction in permeability. Some reduction of permeability in the curve of the 11.1 mm cell was indicated by the fact that ΔP continued to rise faster than its height in the curve. Slopes in the flat vertical regions of Fig. 16 were much greater than for horizontal regions because changes in hydrostatic pressure in the former were comparable to those accompanying increased length of fluid. (Although they are not plotted in Fig. 16, a small pres-

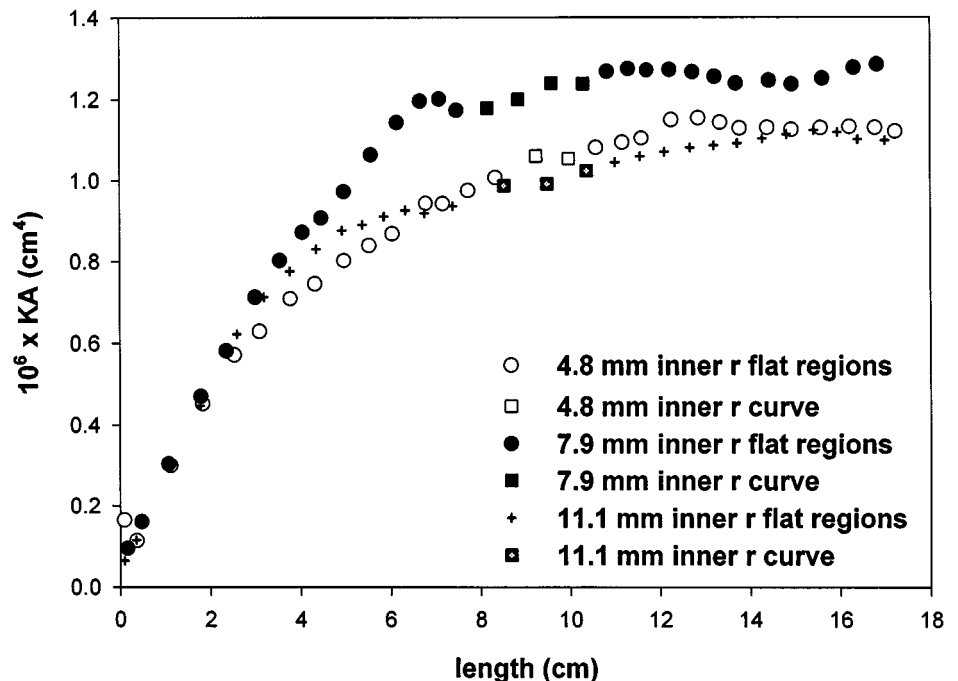


Fig. 15. Cumulative KA vs. average length of the absorption front for the 3-dimensional woven glass fabrics in L -cells with different curvatures with H_2O at $Q = 0.2 \text{ cm}^3/\text{s}$.

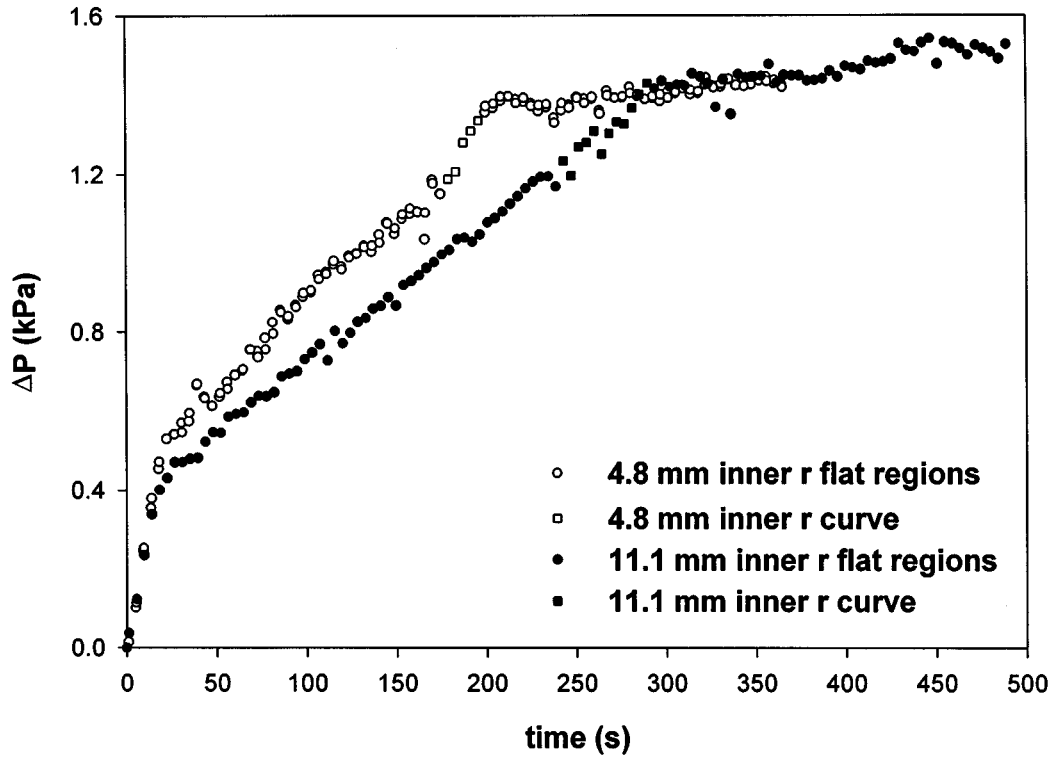


Fig. 16. ΔP vs. time for the 3-dimensional woven glass fabrics in L-cells with different curvatures with H_2O at $Q = 0.02 \text{ cm}^3/\text{s}$.

sure drop was observed when liquid emerged from these fabrics, as for faster flows in Fig. 11. The duration of the measurement in the 4.8 mm cell was shorter and its ultimate pressure drop was smaller than the other because the specimen was shorter.)

Plots of L vs. t (not shown) were nearly linear as they were for faster flows in Fig. 12. Their average velocities in Table 2 were less than $0.1 \times$ those for the same cell at faster flow rates (see Table 1). This was probably due to greater fluid penetration within the

Fig. 17. ΔP vs. time in the vertical region for fast and slow liquid flow for the 3-dimensional woven glass fabrics with H_2O in the L-cell with the 11.1 mm inner radius. (The lines are for regression fits after the initial rapid pressure rise.)

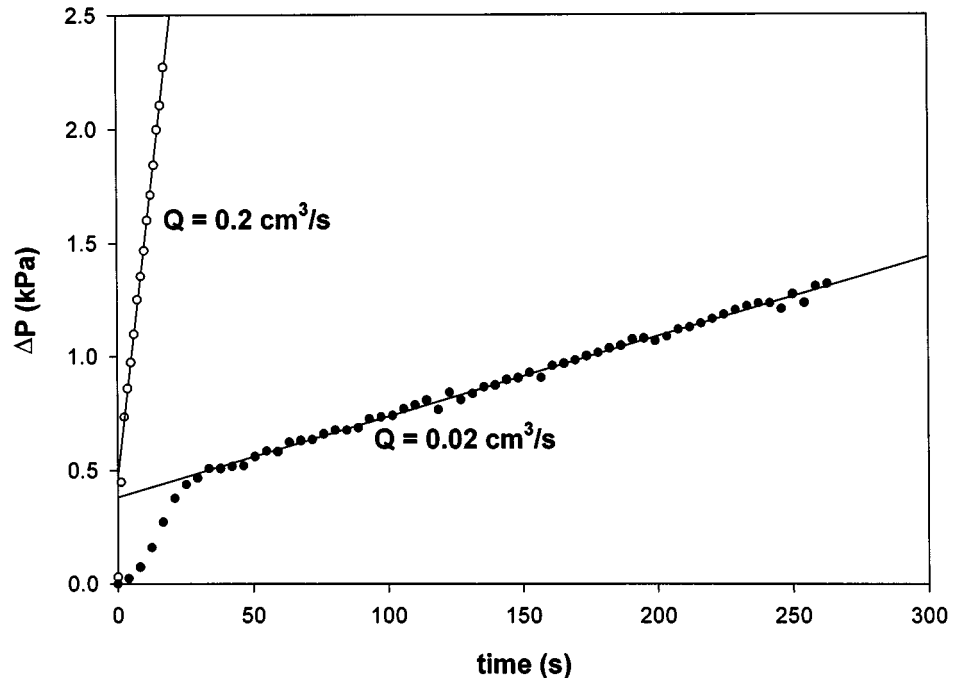


Table 2. Average Linear Liquid Velocities and Permeability Coefficients of 3-Dimensional Woven Glass Fabrics in L-cells With H₂O at Q = 0.02 cm³/s.

Inner Radius, mm	Avg. dL/dt , cm/s	$10^6 \times K_r A$, cm ⁴		$10^6 \times K_t A$, cm ⁴	
		—	—	liquid	air
4.8	0.0448	—	1.06	0.60	1.71
11.1	0.0358	1.44	1.09	0.58	1.37

tows at slower flow rates, consistent with the longer time available for that process. In fact, the average linear velocity in the 11.1 mm cell was approximately that expected for saturated flow. This difference between faster and slower flows was also supported by luminosity measurements, which are described later.

Plots of ΔP vs. L for both of these measurements are shown in Fig. 18, and values of $K_v A$, $K_h A$, and $K_t A$ (determined with Eqs 2, 3, and 7) for liquid and air are shown in Table 2. While superficial characteristics of the plots are similar to Fig. 13, values of $K_v A$ and $K_h A$ are thought to be less accurate than for fast flow (see Table 1). Inaccuracies in the vertical region are a consequence of the fact that values of $d\Delta P/dL$ are nearly the same as ρg (see Eq 3); K_v could not be determined for the 4.8 mm cell because the former was slightly smaller than the latter. Values of $K_h A$ are nearly the same as for fast flow, but they are somewhat arbitrary because linear correlations are very poor. Liquid values of $K_t A$ are about half of those for fast flow or air permeability, probably as a consequence of the inability

to account for the relatively larger contribution of the initial pressure rise for slow flow.

Cumulative values of KA were calculated by use of Eq 8, and are plotted vs. L in Fig 19. Comparison with Fig. 13, shows that permeabilities at comparable lengths were smaller than for faster flow, consistent with greater fluid penetration. Interpolated values in the curve indicate a significant reduction in permeability in the cell with the smaller radius of curvature, compared with the other cell. (Scatter in the curve of the latter is thought to reflect noise in pressure readings.) Cumulative permeabilities continued to increase after liquid was in the flat horizontal region, in contrast to the faster flows in Fig. 13. This suggests that the effect of the initial pressure rise may endure for greater penetration for slower flow. The specific structures of the plots in Fig. 19, near the end of the fabric, are thought to reflect errors in length measurements towards the end of the horizontal region, so we do not know if their permeabilities leveled off before liquid reached the end of the specimen.

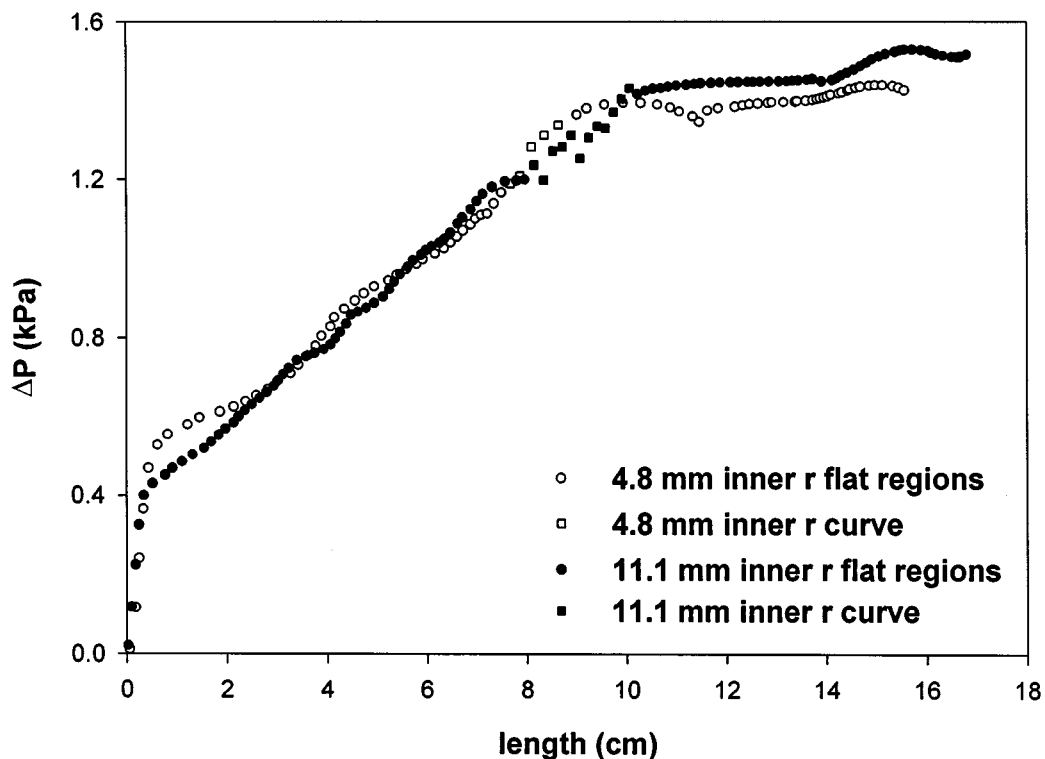


Fig. 18. ΔP vs. average length of the absorption front for the 3-dimensional woven glass fabrics in L-cells with different curvatures with H₂O at Q = 0.02 cm³/s.

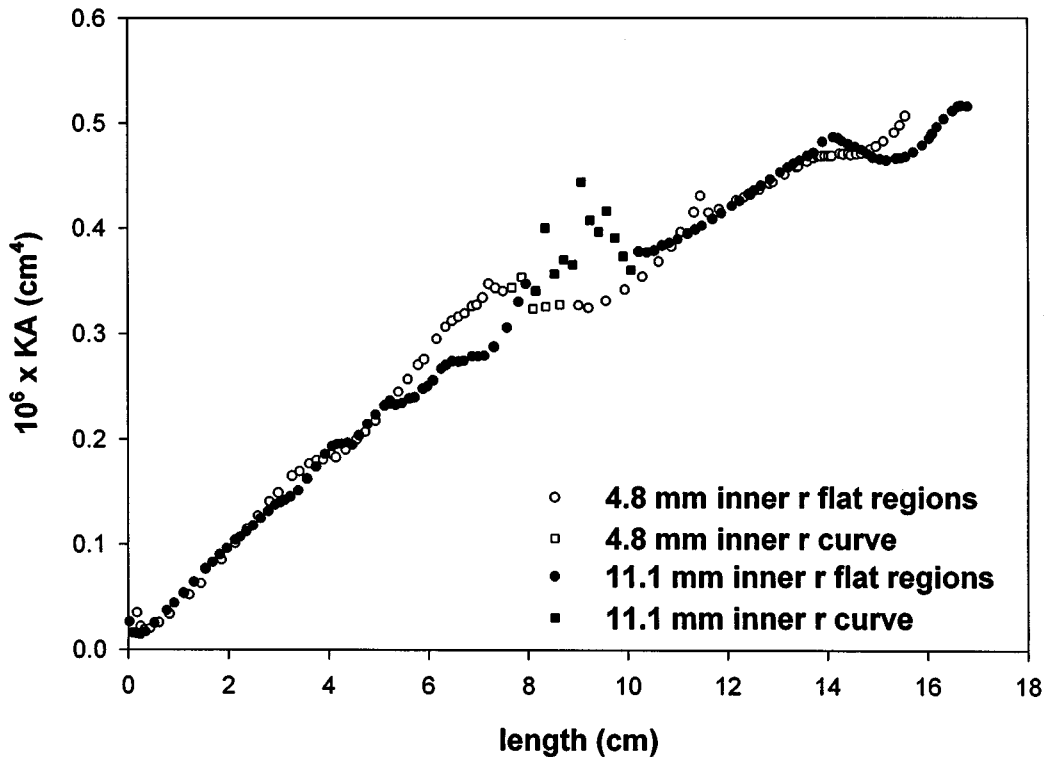


Fig. 19. Cumulative KA vs. average length of the absorption front for the 3-dimensional woven glass fabrics in L-cells with different curvatures with H_2O at $Q = 0.02 \text{ cm}^3/\text{s}$.

Luminosity

A useful insight to fluid penetration in the fabric can be obtained by examining plots of luminosity vs. time. (Reduced luminosity is defined in units of gray scale, in the range of 0 to 255, as total luminosity of the image divided by number of pixels.) Figure 20 shows the typical case of liquid flows of 0.02 and 0.2 cm^3/s in the 11.1 mm cell. When the liquid was injected into the fabric at the slower rate, luminosity of the image reached its maximum level when the front passed the observation area. For faster flow, luminosity continued to increase, but at a slower rate, after the front disappeared. A possible reason for the difference is that only a part of the fabric is initially filled during faster flow, i.e., the relatively large pores between yarns. The smaller voids between filaments are probably filled later. For slower flow, both types of pores seem to be filled at about the same time. This is consistent with the fact that permeability, when calculated from the fluid front displacement, was greater for the faster flows. In principle, the permeability of the fabric behind the liquid front should depend on the extent to which it is filled. Further quantitative analysis of the reduced luminosity as a function of time would help in the analysis of flows in the various locations, including the curve.

DISCUSSION

Measurements and theoretical analysis of the non-woven polyester, show that comparisons of flow in the

flat and curved regions agreed with findings during our earlier studies with the LADA system (12), and testify to the quality of our current measurement system. Thus, in this section, we will only discuss measurements of 3-dimensional woven glass samples, for which we have qualitatively demonstrated that there is a reduction in permeability in the curved regions compared to the flat ones, but are unable to quantify permeability in the curve because we cannot account for the steep initial pressure rise that is a characteristic property of forced flow in this type of fiber network [see Figs. 11, 13, and 16–18 and (2)]. This seems to be an intriguing observation, which was not expected for hydrophilic systems. [Hydrophilicity of the samples was independently proved by wetting force (13) and wicking measurements (3). The results of wicking measurements will be presented elsewhere.]

As shown in Fig. 17, a tenfold reduction in the flow rate led to a proportional reduction in $d\Delta P/dt$ during the initial pressure rise, but there was no significant change in its magnitude. This cannot be explained by the hydraulic resistance of the entrance, which would cause an additional pressure drop proportional to flow rate. We are dealing with a nonlinear effect, which cannot be described in terms of the viscous flow governed by d'Arcy's law. This effect could be related to the formation of an irregular frontal zone during liquid-air displacement. Irregular frontal lines were observed in all of our measurements and are characteristic of the process of such displacement in fiber

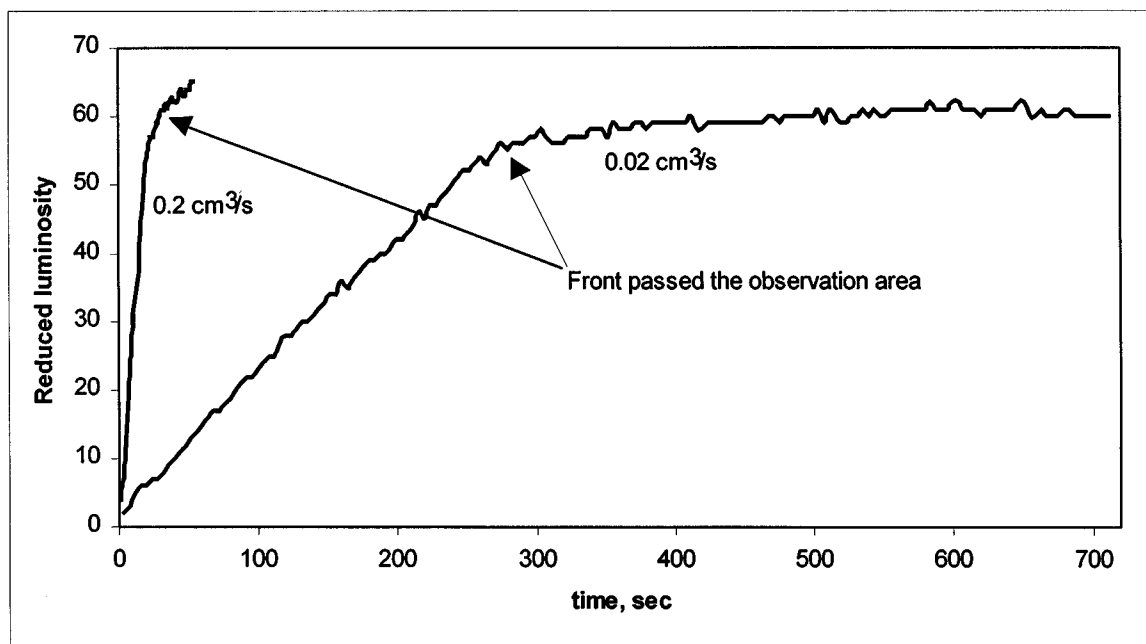


Fig. 20. Image luminosity vs. time for fast and slow liquid flow for the 3-dimensional woven glass fabrics in the L-cell with the 11.1 mm inner radius.

networks. The frontal zone patterns contain liquid fingers, which stick and slip, coalesce and subdivide. At a microscopic level of individual pores, the frontal movement is chaotic and could lead to the small pressure fluctuations shown in *Figs. 11 and 16*. The stick-slip and coalescence-branching effects cause a dissipation in addition to the viscous drag. The energy dissipation in the frontal zone corresponds to an apparent resistance to fluid flow, which contributes to the total effective resistance. We assume that the frontal zone is formed in the beginning of the fluid-solid contact, and then traverses along the sample with the average rate of fluid flow. The frontal zone resistance and associated pressure difference seem to relax in the course of the displacement. Nonlinear behavior of the pressure (corrected for gravity) vs. displacement plot, e.g., in the curved region, implies a restructuring of the frontal zone due to compression effects and corresponding increase of the apparent frontal zone resistance. Structural nonuniformity also can lead to amplifying or damping of the liquid fingers and associated frontal restructuring.

Our measurements were made at low capillary numbers, i.e., $Ca = v\eta/\gamma < 10^{-4}$. The magnitude of Ca characterizes the relation between viscous and capillary forces. In our case, capillarity dominates and governs liquid distribution on a microlevel of inter-fiber pores. This means that the observed frontal irregularities are not related to a phenomenon of viscous fingering. The observed patterning is caused by local heterogeneity of the pore network, and is referred to as capillary fingering. For capillary networks, fingering is described in terms of an invasion percolation model (14). However, pore structures

are complex in fiber networks, and cannot easily be mapped for an effective capillary network.

There are different factors that condition the frontal zone formation and development: nonuniform pore network structure, surface heterogeneity, air entrapment, surface contamination by any impurities, diffusion of surface active components, prewetting of initially dry fibers via flow of precursor films and/or vapor transfer/adsorption, etc.

There is another plausible factor for these fabrics, i.e., competition between the liquid flow between the yarns and the impregnation of the individual fiber bundles. A two stage saturation of the glass samples for faster flow was observed by the luminosity analysis in our visualization studies (see **Luminosity** section).

CONCLUSIONS

We have developed an effective system for controlling and visualizing forced in-plane liquid flow in fabrics. Software developed during this investigation, has the potential to estimate the quantity of liquid at different locations as flow progresses.

For a nonwoven polyester, by applying d'Arcy's law, we were able to quantify permeabilities (calculated from fluid front position) in three contiguous regions with equal gaps, namely a flat vertical region followed by a 90° curve, and finally into a flat horizontal region, permeability was the same in the first and third regions, but was significantly smaller in the curve, consistent with earlier findings by LADA measurements (10).

For the 3-dimensional woven glass fabric, we were not able to quantify permeabilities in all three regions

by applying d'Arcy's law. We seemed to be successful in the third (horizontal) region, but failed in the others, probably because we could not account for an enduring, dominant nonlinear entrance resistance, which was characterized by a pressure rise when liquid contacted the fabric. The magnitude of the rise was independent of flow rate. Apparent permeabilities were significantly larger at $Q = 0.2 \text{ cm}^3/\text{s}$ than at $0.02 \text{ cm}^3/\text{s}$, because not all the pores are initially filled for the faster rate. Presumably, initial flow tends to progress between yarns only at the higher flow rate, and between yarns and fibers during slower flow. There was an apparent reduction in permeability in the curve, in agreement with earlier findings by LADA measurements (10).

ACKNOWLEDGMENT

These studies were supported by the National Institute of Standards and Technology, under Cooperative Agreement No. 70NANB6H0039 and they also form part of TRI/Princeton's project on Interactions of *Fluids With Fibrous Materials*, supported by a group of TRI Corporate Participants.

NOMENCLATURE

A = cross-sectional area of fabric, cm^2
 Ca = Capillary Number = $v\eta/\gamma$
 K = permeability coefficient, cm^2
 K_c = permeability coefficient in the curve, cm^2
 K_h = permeability coefficient in the horizontal flat region, cm^2
 K_t = overall permeability coefficient, cm^2
 K_v = permeability coefficient in the vertical flat region, cm^2
 L = length of fluid front in the fabric, cm
 L_c = length of the curved fabric, cm
 L_h = length of the horizontal flat fabric, cm
 L_t = overall length of the fabric, cm
 L_v = length of the vertical flat fabric, cm
 ΔP = pressure drop along the length of fluid flow, Pa
 ΔP_c = pressure drop along the curve when fluid exits the fabric, Pa
 ΔP_h = pressure drop along the horizontal flat region when fluid exits the fabric, Pa

ΔP_t = overall pressure drop when fluid exits the fabric, Pa
 ΔP_v = pressure drop along the vertical flat region when fluid exits the fabric, Pa
 Q = volumetric flow rate, $\text{cm}^3 \cdot \text{s}^{-1}$
 g = gravitational constant = $98.07, \text{Pa} \cdot \text{cm}^2 \cdot \text{g}^{-1}$
 h = height of the liquid front above the fabric entrance, cm
 h_h = height of the liquid front above the fabric entrance in the horizontal region, cm
 r = radius of the curve, cm
 t = time, s
 v = fluid velocity, $\text{cm} \cdot \text{s}^{-1}$
 γ = fluid surface tension, $\text{Pa} \cdot \text{cm}$
 η = fluid viscosity, $\text{Pa} \cdot \text{s}$
 θ = radial angle between L and L_v when the liquid front is in the curve, deg
 ρ = fluid density, $\text{g} \cdot \text{cm}^{-3}$

REFERENCES

1. R. S. Parnas, in *RTM for Aerospace Applications*, Chap. 8, T. K. Kruckenberg, ed., Chapman & Hall (1998).
2. R. S. Parnas, J. G. Howard, T. L. Luce, and S. G. Advani, *Polym. Compos.*, **16**, 429 (1995).
3. B. Miller and H. L. Friedman, *Nonwovens World*, **2**(3), 83 (1993).
4. R. S. Parnas and F. R. Phelan, *SAMPE Q*, **22**, 53 (1991).
5. R. S. Parnas, K. M. Flynn, and M. E. Dal-Favero, *Polym. Compos.*, **18**, 623 (1997).
6. F. R. Phelan, Y. Leung, and R. S. Parnas, *J. Thermoplastic Compos. Mater.*, **7**, 208 (1994).
7. C. D. Rudd, A. C. Long, P. McGeehin, and P. Smith, *Polym. Compos.*, **17**, 52 (1996).
8. S. Bickerton, P. Simacek, S. Guglielmi, and S. G. Advani, *Composites, Part A*, **28A**, 801 (1997).
9. F. Trochu, A. Hammami, and Y. Benoit, *Composites: Part A*, **27**, 319 (1996).
10. H. L. Friedman, R. A. Johnson, B. Miller, D. R. Salem, and R. S. Parnas, *Polym. Compos.*, **18**, 663 (1997).
11. H. L. Friedman and B. Miller, *Techtextil Symposium 94*, Lecture No. 233, Frankfurt am Main, Germany (June 1994).
12. B. Miller, H. L. Friedman, and M. Körner, *Book of Papers, INDA-Tec 95*, p. 157, St. Petersburg, Florida (September 1995).
13. Y. K. Kamath, C. J. Dansizer, and H.-D. Weigmann, *J. Appl. Polym. Sci.*, 2295 (1978).
14. R. Lenormand, *Proc. R. Soc. London*, **A 423**, 159 (1989).